Journal of Molecular Catalysis A: Chemical 344 (2011) 122–127

Contents lists available at ScienceDirect

Journal of Molecular Catalysis A: Chemical

journal homepage: www.elsevier.com/locate/molcata

Effect of metal–support interaction on the catalytic performance of Ni/Al_2O_3 for selective hydrogenation of isoprene

Rong Wang[a], Yonghong Li[a,b,*], Ronghui Shi[a], Meimei Yang[a]

[a] Key Laboratory for Green Chemical Technology, School of Chemical Engineering, Tianjin University, Tianjin 300072, China
[b] National Engineering Research Center for Distillation Technology, Tianjin University, Tianjin 300072, China

ARTICLE INFO

Article history:
Received 19 January 2011
Received in revised form 22 April 2011
Accepted 15 May 2011
Available online 23 May 2011

Keywords:
Nickel catalysts
Isoprene selective hydrogenation
Metal–support interaction
Coking
Active sites

ABSTRACT

The effect of the interaction between metal and support on the performance of different phases alumina supported nickel catalysts was demonstrated in liquid phase selective hydrogenation of isoprene in simulated gasoline. Catalysts supported on γ-Al_2O_3 and κ-Al_2O_3 were characterized by BET, XRD, TPR, and XPS techniques. The results showed that a "surface spinel", $NiAl_2O_4$ was formed. The supported nickel ions preferentially incorporate into the tetrahedral vacancies of γ-Al_2O_3 support to form SMSI (strong metal–support interaction), while WMSI (weak metal–support interaction) was formed on κ-Al_2O_3 support with little tetrahedral vacancy. When there were enough hydrogenation sites, the Ni/γ-Al_2O_3 catalysts with SMSI which can resist carbon deposition, performed higher isoprene conversion, higher stability and lower selectivity than the same nickel loading Ni/κ-Al_2O_3 samples with WMSI. The weak interaction had a positive effect on the formation of coke, which was mainly related to the hydrogenolytic sites, leading to main reaction with high mono-olefins selectivity with isoprene conversion decrease evidently.

1. Introduction

Selective hydrogenation of highly unsaturated hydrocarbons into the corresponding mono-olefins is an important segment of commercial catalytic hydrogenations in the petrochemical and fine chemical industries [1,2]. Nickel-based catalysts, with low-cost and long-proven performance, would be optimized for hydrogenation applications, particularly for fuel processing from existing liquid fuels such as gasoline and diesel [3,4].

Ni/Al_2O_3 catalyst has received much attention since the pioneering work by Hill and Selwood [5] in 1949. Ni^{2+}, occupying the octahedral and tetrahedral sites of alumina, formed "surface spinel". SMSI (strong metal–support interaction) has been proven to enhance Ni dispersion and reduce Ni crystal size, which will prevent the large Ni clusters forming during catalyst preparation and activation [6,7]. Chary et al. [8] studied nickel-based catalysts supported on different alumina phases [γ, ($\gamma+\theta$), ($\theta+\alpha$), α]. The study indicated that the loss of surface hydroxyl groups on alumina supports, resulted from the increase in calcinations temperature, and diminished metal–support interaction.

In general, the selective hydrogenation studies, over nickel-based catalysts with different preparation and activation conditions, have been typically carried out for hydrogenation of ethyne or 1,3-butadiene [9–11], though other alkynes and dienes have been also studied [3,12–14]. However, it seems that the evaluation of the effect of the interaction of nickel oxide and different alumina phases on the catalytic performance in selective hydrogenation of diene has not been reported. Besides which, studies assessing the relationship between SMSI and hydrogenation active sites of nickel catalyst have received much less attention.

In this work, we have studied the physicochemical properties of nickel-based catalysts supported on γ- and κ-phase alumina by a series of characterization methods, and investigated the influence of metal–support interaction on the catalytic performance of Ni/Al_2O_3 in selective hydrogenation of isoprene. Moreover, we also attempted to correlate SMSI with the active sites of these catalysts for isoprene hydrogenation.

2. Experimental

2.1. Catalyst preparation and activation

The γ-Al_2O_3 and κ-$A1_2O_3$ support were obtained by calcinations of $Al(OH)_3$ at 973 K and 1273 K, respectively. The catalysts precursors were prepared by wetness impregnations, followed by drying at 393 K overnight and calcinations at 823 K for 4 h.

* Corresponding author at: Key Laboratory for Green Chemical Technology, School of Chemical Engineering, Tianjin University, Tianjin 300072, China.
Tel.: +86 22 87898607; fax: +86 22 27403389.
E-mail address: yhli@tju.edu.cn (Y. Li).

1381-1169/$ – see front matter © 2011 Elsevier B.V. All rights reserved.
doi:10.1016/j.molcata.2011.05.009

Before the catalytic tests (Section 2.3), the calcined samples were treated in H_2. In this work, calcined and reduced samples were designated as 'C-x-y' and 'R-x-y', respectively, where 'x' and 'y' stood for alumina polymorph and nickel loading.

2.2. Catalyst characterizations

The surface areas of calcined samples were measured by N_2-BET with a Micrometrics ASAP 2010 instrument. Pore size distribution was determined from the isotherm desorption branch by the BJH formula.

X-ray diffraction (XRD) patterns were obtained with a Rigaku D/MAX-2500 diffractometer with Cu Kα radiation (40 kV, 100 mA).

Temperature-programmed reduction with hydrogen (H_2-TPR) was measured in a Micrometric AutoChem 2910 unit. Ca. 50 mg sample was loaded in the quartz microreactor, treated in Ar atmosphere at 573 K for 60 min, and cooled to room temperature in the same atmosphere. The analysis was carried out in the H_2/Ar (ratio of 1/19), ramping the temperature to 1173 K at 10 K min^{-1}. TPO was carried out by using the Microreactor system to determine consisted carbon species on the catalysts after 10 h stability tests. Experiments were carried in a gas mixture of 3% O_2/Ar (40 ml min^{-1}) over 50 mg of catalyst samples. Temperature was linearly increased from 50 °C to 900 °C at a heating rate of 10 °C min^{-1}.

X-ray photoelectron spectra (XPS) analysis was acquired on a Perkin-Elmer PHI-1600 ESCA spectrometer using Mg Kα radiation (1253.6 eV). Binding energies were calibrated relative to the C1s peak from carbon contamination at 284.6 eV. The introduction chamber of the spectrometer was located in a glove box for the preparation of the reduced samples, which were transferred under inert atmosphere.

2.3. Catalytic tests

Selective hydrogenation of isoprene was carried out with 1.5 g calcined sample loaded in a high pressure stainless steel fixed bed reactor (8 mm i.d.). The loaded sample was pre-reduced by H_2 at 773 K (C-γ samples) or 723 K (C-κ samples) for 4 h. Flow rate of simulated gasoline passing through the catalyst bed in the reactor was controlled by liquid pumps. The reaction was studied with a weight/hourly space velocity (WHSV) of 20 h^{-1} at 80 °C.

The simulated gasoline consisted of 85 wt% n-heptane, 10 wt% isopentene (2-methyl-2-butene: 89%; 2-methyl-1-butene: 11%) and 5 wt% isoprene. Hydrogenation products were withdrawn in half hour intervals from the outlet of the reactor and analyzed by a gas chromatograph equipped with a flame ionization detector (FID, Column OV-101: 60 m × 0.25 mm × 0.50 μm).

Activity and selectivity of Ni/Al_2O_3 were defined as follows:

$$X_{\text{isoprene}} = \frac{\text{moles of isoprene converted}}{\text{moles of isoprene in the feed}} \times 100\% \quad (1)$$

$$S_{\text{mono-olefins}} = \frac{\text{moles of mono-olefins} - \text{moles of isopentene in the feed}}{\text{moles of isoprene converted}} \times 100\% \quad (2)$$

3. Results and discussion

3.1. Characterization of catalysts

3.1.1. BET specific surface

Table 1 lists characterization data of calcined and reduced samples. The γ-Al_2O_3 support with higher surface area (208 m^2/g) than κ-Al_2O_3 (41 m^2/g) was propitious to disperse the active species. BET area decreased with increasing nickel loading. It might have been caused by the blocking of support pores with NiO crystallites, according to the evidence of pore size and following XRD analysis.

Table 1
Characterization data of calcined and reduced sample.

Sample	BET (m^2/g)	Pore size (10^{-10} m)	Sample	Ni^0 crystal size (nm)
C-γ-10	104.5	92.3	R-γ-10	–
C-γ-20	68.3	90.1	R-γ-20	4.4
C-κ-5	37.9	212.5	R-κ-5	3.3
C-κ-20	21.8	171.1	R-κ-20	9.8

3.1.2. XRD studies

XRD patterns of calcined and reduced samples are shown in Fig. 1. The major diffraction features, over the support calcined at 973 K, are characteristic of γ-Al_2O_3 while these over the support, calcined at 1273 K, are κ-Al_2O_3. $NiAl_2O_4$ and NiO are not definitely distinguished by the diffraction features, especially for Ni/γ-Al_2O_3 with overlapping diffraction lines of γ-Al_2O_3. The XRD patterns of reduction samples clearly show the presence of metallic nickel as expected cubic Ni^0. The mean particle size calculated by Scherrer for the (1 1 1) reflection of Ni^0 was lower in R-γ samples, as 4.4 nm for R-γ-20 and 9.8 nm for R-κ-20 (Table 1). It indicated that the samples supported on γ-Al_2O_3 with the larger specific surface had smaller particle size, better dispersions and stronger interaction between metal and support [15], which could be confirmed by TPR and XPS analyses.

3.1.3. TPR studies

Fig. 2 shows the TPR profiles of calcined samples. Pure NiO typically displays a single consumption peak at 673 K, matching the low-temperature peak in C-γ-25 and C-κ samples. The reduction of nickel in $Ni(Al)O_x$ solid solutions is hindered by aluminum, causing the shift to higher temperature [16]. Two peaks of C-γ-5 at 923 K and 1025 K are assigned to free NiO interacting weakly with alumina, and a complex NiO species interacting strongly with alumina, respectively [17]. The puny peak assigned to free NiO at 693 K can be seen in C-γ-15, which would be corresponding to full monolayer coverage [18]. Ni^{2+} preferentially incorporates into the tetrahedral vacancies of Al_2O_3 at low nickel loading, and the ratio of Ni^{2+} occupying the octahedral vacancies of γ-Al_2O_3 increases with increased nickel loading. Each peak shifts to lower temperature with nickel loading increasing, which greatly leads to metal–support interaction diminishing. The lack of free hydroxyl groups and vacancies in κ-alumina leads to WMSI without tetrahedral configurations formation [8]. It was found that each of the five C-κ samples (Fig. 2b) only had two peaks assigned to NiO and octahedral spinel configurations. The intensity of the first peak associated with NiO increases gradually, and it plays a dominant role when nickel loading increased to 20%.

3.1.4. Surface analyses

XPS peaks corresponding to Ni 2p3/2 core electrons energy (around 856.0 eV) can be divided into four subpeaks: 852.9 eV (Ni^0) [19], 854.0 eV (Ni^{2+} in NiO) [20], 855.8 eV (Ni^{2+} in octahedral coordination sites) [21], and 858.2 eV (Ni^{2+} in tetrahedral coordination sites) [21,22] with the corresponding shake-up satellite at ca. 6 eV above the principal line. Characteristic peaks of octahedral and tetrahedral configuration can be found in C-γ-10 (Fig. 3). Ni^{2+} occupying tetrahedral sites preferentially could be overlaid by surface octahedral configuration or NiO species in C-γ-20. In agreement with TPR results, there is no characteristic peak of tetrahedral configuration on the surface of C-κ samples. The XPS spectrum

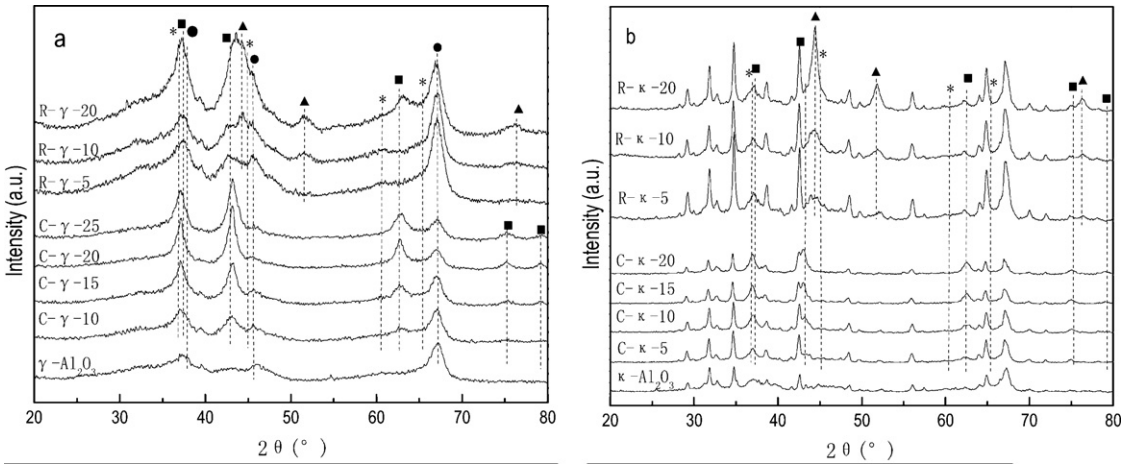

Fig. 1. XRD patterns of supports and the products of calcination and reduction. Crystalline phases: (*) $NiAl_2O_4$, (▲) Ni^0, (■) NiO, (●) γ-Al_2O_3.

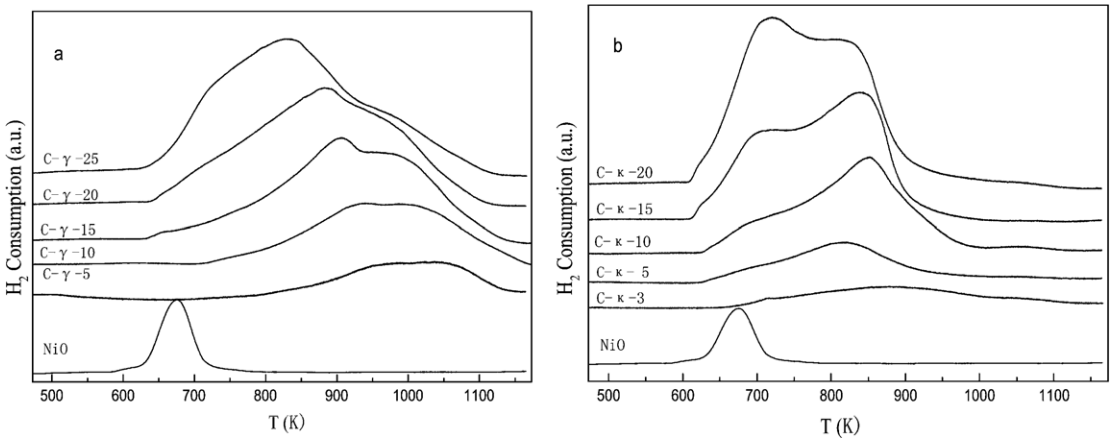

Fig. 2. H_2-TPR profiles of calcined Ni/Al_2O_3 catalysts with different nickel loading.

of reduced sample displays an additional peak assigned to Ni^0, although the peak corresponding to Ni^{2+} in octahedral sites is still predominant. Both κ- and γ-Al_2O_3 are occupied by tetrahedral and octahedral interstitial sites, with many defects such as O^{2-} vacancies in the Al_2O_3 lattice [23]. Ni^{2+} can occupy Al vacancies (in either octahedral or tetrahedral configurations) at proper temperature, leading to the formation of Ni–Al surface spinel. Ni^{2+} will easily incorporate into the tetrahedral sites of γ-Al_2O_3 with more numerous vacant tetrahedral sites to form surface spinel [15].

By peak deconvolution, it was determined that only 31.3% of the nickel probed was in metallic form on R-κ-20 surface. This was much lower than that of 84.3% determined in bulk by H_2-TPR. The same results were obtained in R-γ-20 (22.8% vs 71.7%), which was confirmed by molar Ni/Al ratio in Table 2. It can be

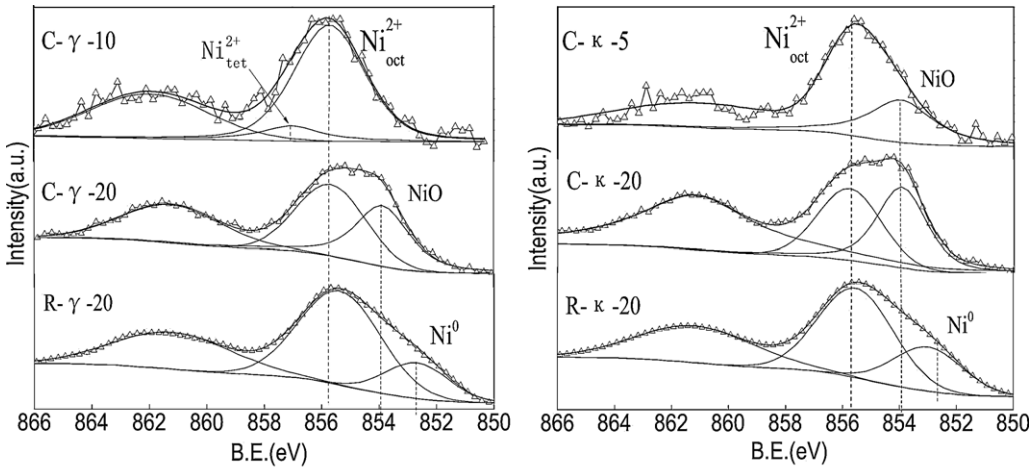

Fig. 3. Ni 2p3/2 core lever spectrum of the catalysts.

Table 2
Comparative results of bulk and surface analyses over selected samples.

Sample	Molar Ni/Al ratio		Ni reduction degree (%)	
	Bulk	Surface (XPS)	Bulk (H_2-TPR)	Surface (XPS)
C-γ-20	0.43	0.18	–	–
R-γ-20	0.43	0.07	71.7	22.8
C-κ-20	0.43	0.27	–	–
R-κ-20	0.43	0.12	84.3	31.3

Table 3
Comparison of surface atomic compositions from XPS analysis.

Atom	Atom ratio (%)			
	R-γ-20		R-κ-20	
	Fresh	Used	Fresh	Used
C	28.8	30.1	28.4	33.9
O	45.3	45.1	44.9	41.8
Ni	1.7	0.8	2.9	1.6
Al	24.1	23.9	23.7	22.6

tentatively explained by the migration of Ni from surface into the bulk forming alumina nickel aluminate with interaction between metal and support, and the progressive coverage of Ni species with some mobile Al that could exist on the support surface which can be observed in TPR profile [10,24]. The sintering of nickel at the surface under a reducing atmosphere is another factor, and it could explain the observed decrease in exposed surface nickel and the increased proportion of Ni^0.

3.1.5. Characterization of surface carbonaceous deposits

Table 3 presents the surface compositions for the fresh and used 20% Ni/Al_2O_3 catalysts. For two kinds of fresh catalysts, carbon content is almost the same. But after reaction, the increased carbon amount for $Ni/\kappa\text{-}Al_2O_3$ is higher than that for $Ni/\gamma\text{-}Al_2O_3$. The characteristics of deposited coke were studied using the temperature-programmed oxidation (TPO) technique. The results in Fig. 4 reveals two types of coke at least on catalyst surface, the lower temperature peak has been attributed to amorphous or monoatomic carbon [25–27], and the new higher temperature peak over R-κ-20 is assigned to nickel carbide or filamentous carbon [28]. For further confirmation the types of coke, the XPS spectra of these Ni/Al_2O_3 catalysts in C1s region are showed in Fig. 5. For two fresh catalysts, the prominent peaks are both at a binding energy of ~284.6 eV in the spectra, which are attributed to the adventitious carbon. The other small peaks at a binding energy of 288.60 eV may be from the residual CO_3^{2-}. After reaction, a small new peak appears at binding energy of 283.3 eV on both catalysts, which could be attributed to amorphous coke [29,30]. But for the used $Ni/\kappa\text{-}Al_2O_3$, another new peak appeared at a binding energy of 281.3 eV, attributed to metal carbide species NiC_x [29]. Obviously $Ni/\gamma\text{-}Al_2O_3$, has better anti-carbon deposit ability than $Ni/\kappa\text{-}Al_2O_3$. The similar phenomenon over Pd catalysts was observed by Chou and co-workers [31]. This could be explained by the high dispersion with small Ni particles promoting the adsorption of isoprene on Ni sites and inhibiting the diffusion of isoprene for further coke formation.

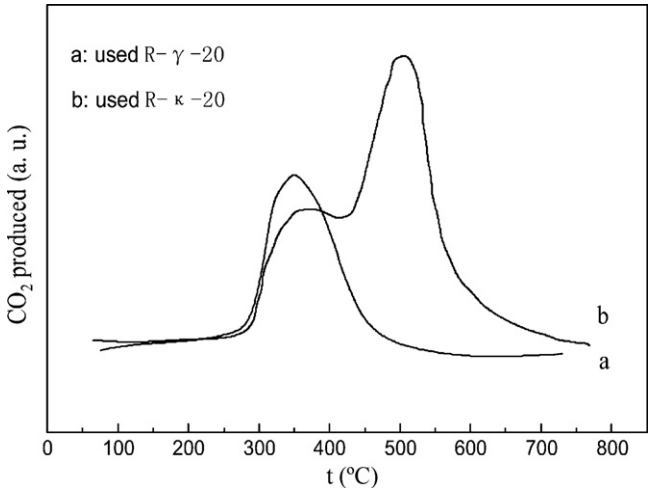

Fig. 4. TPO profiles of Ni/Al_2O_3 samples after reaction10 h.

3.2. Hydrogenation of isoprene

3.2.1. Effect of nickel loading on different alumina phases

Fig. 6 presents the catalytic activities and selectivities of total mono-olefins over nickel-based catalysts. The conversion of isoprene over $Ni/\gamma\text{-}Al_2O_3$ increases with nickel loading increasing until reach a steady state value while the selectivity of total mono-olefins decreases. As a facile reaction, hydrogenation of isoprene depends directly on the thermodynamically stable monolayer metal on the catalyst surface. Therefore, the catalyst with active NiO loading around monolayer dispersion threshold has good performance [18]. It shows that the conversion of isoprene reached a plateau when the nickel loading exceeds 17.5%, which is identical with the monolayer dispersion threshold value of NiO over $\gamma\text{-}Al_2O_3$ [18]. On the catalyst surface, isoprene absorbs more strongly than isopentene and competes with isopentene for hydrogenation sites. Isoprene promotes desorption of isopentene on catalyst surface without sufficient number of hydrogenation active sites when the conversion is low, leading to a high selectivity for mono-olefins.

Unlike $Ni/\gamma\text{-}Al_2O_3$, there is an optimal conversion of isoprene and a corresponding minimum selectivity of mono-olefins over $Ni/\kappa\text{-}Al_2O_3$. The catalyst has much higher conversion of isoprene and lower selectivity of mono-olefins than R-γ at low nickel loading. It can be explained by the smaller specific surface area, lower dispersion capacity of the support, which leads to smaller monolayer dispersion threshold. Therefore, there are enough active sites on surface for isopentene hydrogenation toward isopentane leading to a lower selectivity of mono-olefins. However, the R-κ catalyst performs with higher mono-olefins selectivity and moderate activity than R-γ at the higher nickel content. As mentioned previously, distributed multiplayer resulted in sintering of NiO which can thin out the exposed active sites leading lower hydrogenation activity.

Another parameter may be the formation of C-containing deposits, whose electron-donor character may supply nickel electron density and thereby decreases overlap between d-orbital of surface Ni atoms and π-orbital of isoprene [32]. The electronic effect decreases the affinity of Ni to isoprene causing some active sites deactivation and mono-olefins selectivity enhancement. It could be found in the C1s XPS spectra of used catalysts (Fig. 5), the C-containing deposits with time on stream could promote the reaction selectivity [33].

Additionally, formation of $NiAl_2O_4$ in hydrogenation catalysts has shown high resistance to deactivation by coke formation [34]. Thus the carbonaceous deposits on the surface would perform a major role in the selectivity of mono-olefins when there are enough hydrogenation sites (nickel loading ≥17.5%). The higher conversion of isoprene and lower selectivity of mono-olefins resulted from the presence of $NiAl_2O_4$ with SMSI in R-γ samples.

3.2.2. MSI and active sites

To evaluate the effects of MSI over different alumina supports and coke deposition on the catalytic performance, the catalysts with 20% nickel loading were studied. The catalytic activities of

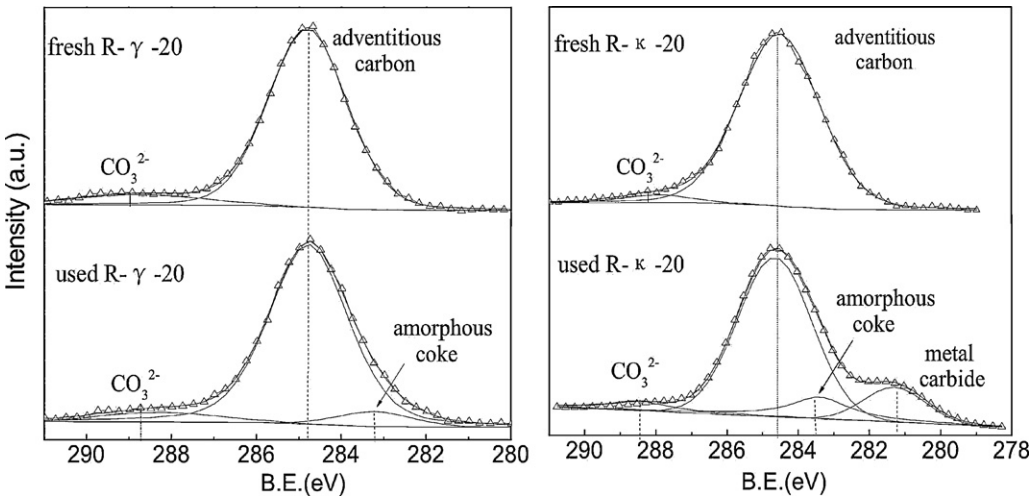

Fig. 5. C1s XPS spectrum of fresh and used 20% Ni/Al_2O_3 catalysts.

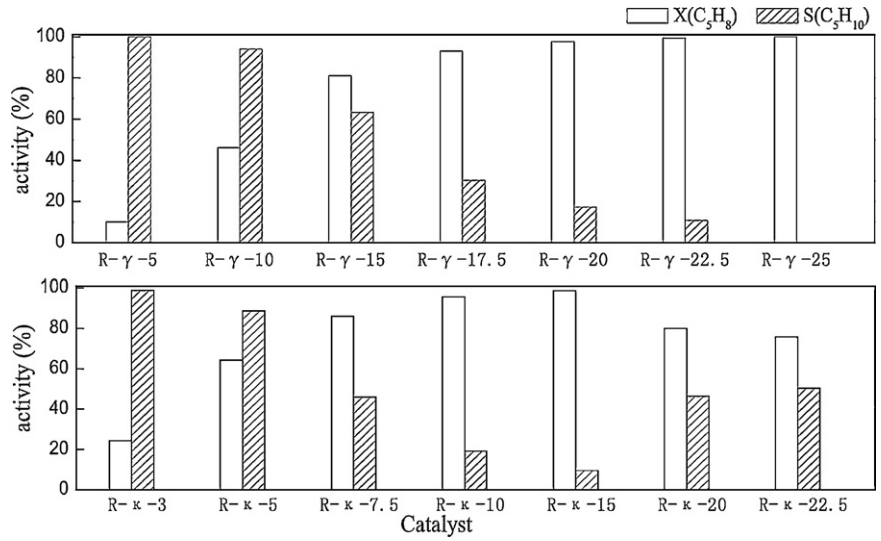

Fig. 6. Isoprene conversion and mono-olefins selectivity over different catalysts conditions: H_2/isoprene ratio = 2, T = 353 K, WHSV = 20 h^{-1}, P = 1.0 MPa.

these catalysts were shown in Fig. 7. There is a sharp increase in the rate of mono-olefins within 150 min to a higher level (a fast decrease in the rate of isopentane simultaneously not shown here). At the early stages of the reaction, a large amount of isopentane is formed. The active sites are quickly deactivated and the isopentane formation rate decreases sharply, a low activity remaining. While main hydrogenation rates reaches relatively stable values by long reaction periods. This suggests that different types of sites may be involved in the two types of reaction. Monzón [33,35] reported these active sites in the nickel catalyst by kinetic model of coke growth: hydrogenolytic (leading to the alkane) and hydrogenating (leading to the alkene) sites, the former sites experiencing a fast deactivation by coke in hydrogenation. Therefore the coke deposition is consistent with the interaction between nickel and support.

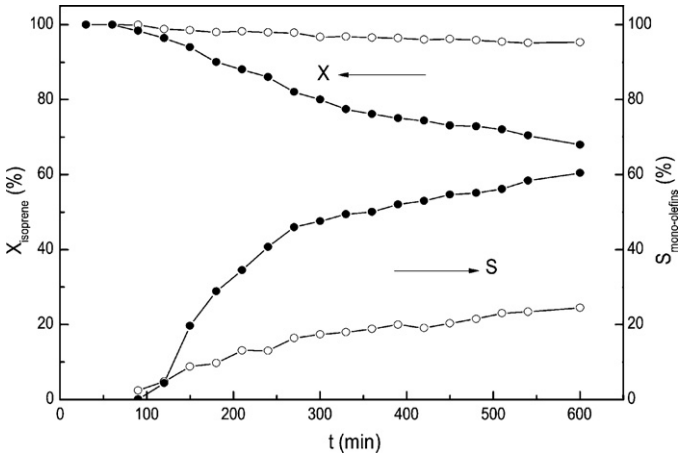

Fig. 7. Catalytic performance of Ni/Al_2O_3 with the time on stream (○ R-γ-20, ● R-κ-20).

For the R-γ-20 sample that is only covered by amorphous coke (Fig. 5), isoprene conversion reaches a plateau quickly and the mono-olefins selectivity increases slightly with time. However, with more coke deposition on surface, especially the metal carbide formation, the R-κ-20 does not present the exactly same behavior. The conversion of isoprene decreases significantly with time. It is consistent with the stronger interaction between nickel and the γ-Al_2O_3 support, and also with the better dispersion of reduced nickel and thus the higher amount of surface metallic nickel. Indeed, the SMSI over R-γ-20 can hinder coke formation and sustain the stability of the catalyst. But for R-κ-20, the larger amount of coke formation favours the mono-olefins formation. The hydrogenolytic sites were covered by metal carbide resulted from weak or little

interaction between nickel and alumina support, as already shown by the XPS and TPR data. Therefore the coke generated restrains the side reaction and the activity of main reaction decreases slightly, too.

Recently, it has been reported that subsurface H strongly enhances total hydrogenation of acetylene. Carbon (from fragmented feed molecules) occupying interstitial lattice sites forms a metastable surface Pd-C species which turns the hydrogenation selective [36].

Based on these results, it is plausible that nickel hydride-type species superimposed on the (sub-)surface are hydrogenolytic sites favorable to total hydrogenation. These sites can be deactivated easily by C-containing deposits especially metal carbide, associated with octahedral spinel configurations with WMSI. However, tetrahedral configurations with SMSI could suppress the coke deposits. The hydrogenating sites, deactivated by amorphous coke species on the surface, are active for the main reaction. When the hydrogenolytic sites are relatively quickly self-deactivated by coke [34] such as metal carbide species, the predominant reaction will be selective hydrogenation with high mono-olefins selectivity. Further studies about the unclear structure and nature of these species are required to ascertain the active hydrogenation sites.

4. Conclusions

Reduced nickel-based catalysts supported on alumina are highly active and selective catalysts for partial hydrogenation of isoprene without addition of promoters. As the alumina phase and metal content determine the nature of the catalysts, proper selection of these factors is decisive for the catalytic behavior, especially for the mono-olefins selectivity affected by metal–support interaction. The results show that NiO in the γ-Al_2O_3 matrix is more interdispersed than that of κ-Al_2O_3 matrix. Thus the interaction of these particles with the matrix is stronger in Ni/γ-Al_2O_3, and metallic nickel particles are smaller than these in κ-Al_2O_3. Extensive sintering of NiO at high nickel loading in Ni/κ-Al_2O_3 induces lower activity comparatively, while crystallization of $NiAl_2O_4$ (tetrahedral sites) in Ni/γ-Al_2O_3 leads to lower C-containing deposition and lower selectivity of mono-olefins. SMSI results in amorphous coke which deactivates the hydrogenating sites which are active for main reaction, while metal carbide formed with WMSI covers hydrogenolytic sites, active for the side reaction total hydrogenation.

Acknowledgements

This project was supported by Fund of National Natural Science Foundation of China (No. 20976129) and the Program of Universities' Innovative Research Terms (No. IRT0936).

References

[1] Á. Molnár, A. Sárkány, M. Varga, J. Mol. Catal. A 173 (2001) 185–221.
[2] K. Pattamakomsan, K. Suriye, S. Dokjampa, N. Mongkolsiri, P. Praserthdam, J. Panpranot, Catal. Commun. 11 (2010) 311–316.
[3] F. Alonso, I. Osante, M. Yus, Tetrahedron 63 (2007) 93–102.
[4] D.L. Trimm, I.O.Y. Liu, N.W. Cant, Appl. Catal. A: Gen. 374 (2010) 58–64.
[5] F.N. Hill, P.W. Selwood, J. Am. Chem. Soc. 71 (1949) 2522–2529.
[6] B.S. Liu, C.T. Au, Appl. Catal. A: Gen. 244 (2003) 181–195.
[7] L. Znak, J. Zielinski, Appl. Catal. A.: Gen. 334 (2008) 268–276.
[8] K.V.R. Chary, P.V.R. Rao, V.V. Rao, Catal. Commun. 9 (2008) 886–893.
[9] P.B. Wells, G.R. Wilson, J. Chem. Soc. A (1970) 2442–2447.
[10] S. Abelló, D. Verboekend, B. Bridier, B. Bridier, J. Pérez-Ramírez, J. Catal. 259 (2008) 85–95.
[11] B. Bridier, N. López, J. Pérez-Ramírez, J. Catal. 269 (2010) 80–92.
[12] F. Alonso, M. Yus, Tetrahedron Lett. 37 (1996) 6925–6928.
[13] F. Alonso, M. Yus, Tetrahedron Lett. 38 (1997) 149–152.
[14] F. Alonso, I. Osante, M. Yus, Adv. Synth. Catal. 348 (2006) 305–308.
[15] M. Lo Jacono, M. Schiavello, A. Cimino, J. Phys. Chem. 75 (1971) 1044–1050.
[16] O. Clause, M. Gazzano, D. Matteuzzi, F. Trifiro, A. Vaccri, J. Catal. 133 (1992) 231–246.
[17] J. Hu, J.A. Schwarz, Y.J. Huang, Appl. Catal. 51 (1989) 223–233.
[18] Y.C. Xie, Y.Q. Tang, Adv. Catal. 37 (1990) 1–43.
[19] F.V. Looij, J.W. Geus, J. Catal. 168 (1997) 154–163.
[20] A.N. Mansour, Surf. Sci. Spectra 3 (1996) 239–246.
[21] G. Poncelet, M.A. Centeno, R. Molina, Appl. Catal. A: Gen. 288 (2005) 232–242.
[22] F. Loviat, I. Czekaj, J. Wambach, A. Workun, Surf. Sci. 603 (2009) 2210–2217.
[23] Y.J. Huang, J.A. Schwarz, Appl. Catal. 37 (1988) 229–245.
[24] I. Czekaj, F. Loviat, J. Wambach, A. Wokaun, Chimia 63 (2008) 193–196.
[25] S. Wang, G.Q. Lu, Appl. Catal. B 19 (1998) 267–277.
[26] D.L. Trimm, Catal. Today 49 (1999) 3–10.
[27] L. Kepinski, B. Stasinska, T. Borowiecki, Carbon 38 (2000) 1845–1856.
[28] Y.X. Pan, C.J. Liu, P. Shi, J. Power Source 176 (2008) 46–53.
[29] I. Czekaj, F. Loviat, F. Raimondi, Appl. Catal. A: Gen. 329 (2007) 68–78.
[30] J.G. Wang, C.J. Liu, Y.P. Zhang, K.L. Yu, X.L. Zhu, F. He, Catal. Today 89 (2004) 183–191.
[31] J.-C. Chang, T.-C. Chou, Appl. Catal. A: Gen. 156 (1997) 193–205.
[32] J.B. Branco, A.P. Goncalves, A.P. Mato, J. Alloys Compd. 465 (2008) 361–366.
[33] C. Guimon, A. Auroux, E. Romeo, A. Monzón, Appl. Catal. A: Gen. 251 (2003) 199–214.
[34] J.A. Pena, J. Herguido, C. Guimon, A. Monzón, J. Santamada, J. Catal. 159 (1996) 313–322.
[35] A. Monzón, E. Romeo, C. Royo, R. Trujillano, F.M. Labajos, V. Rives, Appl. Catal. 185 (1999) 53–63.
[36] D. Teschner, J. Borsodi, A. Wootsch, Z. Révay, M. Hävecker, A. Knop-Gericke, S.D. Jackson, R. Schlögl, Science 320 (2008) 86–89.